Joint Special Interest Group meeting between euspen and ASPE
Advancing Precision in Additive Manufacturing
Ecole Centrale de Nantes, France, September 2019
www.euspen.eu

Automated characterisation of multi-view fringe projection system for three-dimensional measurement of additively manufactured parts

A. Shaheen, D. Sims-Waterhouse, P. Bointon, S. Piano, R. K. Leach

Manufacturing Metrology Team, Faculty of Engineering, University of Nottingham, UK

amrozia.shaheen1@nottingham.ac.uk

Abstract

Digital fringe projection is a non-contact method that is widely used for the dimensional characterisation of complex manufactured parts. However, single camera-projector fringe projection systems struggle to acquire the full three-dimensional point cloud in one acquisition due to their relatively small field-of-view, and the typically freeform geometry, potentially with multiple occlusions, of additively manufactured parts. In this paper, we demonstrate that a multi-view fringe projection system is an effective solution to address form measurement of complex additively manufactured parts. However, the global geometric characterisation of multiple sets of cameras and projectors is a challenge due to the lack of a common field-of-view and overlapping of the projected fringes. We use a cost-effective multi-view fringe projection system to characterise an assembly of multiple sets of cameras and projectors with different perspectives. We present an automated characterisation method that uses a checkerboard which is moved in the measurement volume. The absolute phase information from the captured phase-stepped images is used to establish the global geometric properties by automated image processing and parameter optimisation. The geometric characterisation method is implemented and the multi-view system has been used to measure a range of additive parts. In this paper, we present the three-dimensional reconstruction results from different views that are combined to optimise the global geometric parameters.

Keywords: Form, Metrology, Automation, Reconstruction

1. Introduction

Digital fringe projection (DFP) is an optical method that is extensively used in three-dimensional shape measurement due to its fast acquisition rates, non-contact and non-destructive nature [1-3]. DFP has been used in a variety of applications, such as manufacturing quality control [5], biomedical [6], and reverse engineering [7]. Current fringe projection systems based on a single camera-projector pair have some limitations in acquiring the three-dimensional form in one acquisition due to the small field-of-view of the camera, the frequent presence of occlusions and high slope angles of the freeform geometries of additively manufactured (AM) parts. A possible solution to overcome these limitations is to introduce multiple cameras and projectors to acquire multiple views.

In DFP systems, geometric characterisation is the first and critical step which has a decisive influence on the system performance. System geometric characterisation involves the determination of both the intrinsic and extrinsic properties of both the cameras and projectors within the system [8-9]. In DFP systems, the camera intrinsic and extrinsic parameters are determined which are then used to deduce the projector parameters. However, with this methodology, errors in the camera characterisation will be inferred to the projector characterisation, decreasing the accuracy of the DFP system.

Generally, the geometric characterisation of a multi-view system is a challenge, as it requires a global frame of reference for all the cameras and projectors. A common approach is the extension of the single camera-based method proposed by Huang et al. [12] and Zhang et al. [13]. With this method, each camera is characterised with a planar target and then the location relationship between the different views is obtained by global optimisation of location parameters of all the views.

In this paper, we present the geometric characterisation method of a cost-effective multi-view fringe projection system for complex form measurement. The method involves an integrated characterisation target (checkerboard), automated image acquisition and image processing technique and parameter optimisation. We demonstrate the geometric characterisation technique by determining the global world coordinate system and combining the three-dimensional reconstruction results from different perspectives. The characterisation results are implemented, and the multi-view fringe projection system is tested to acquire the three-dimensional shape of a (60 × 60 × 20) mm, Nylon-12 AM part. The 3D reconstructions from different perspectives are aligned with the computer-aided design (CAD) model and finely registered with an iterative closest point (ICP) algorithm [17].

2. Methodology

The multi-view fringe projection system is comprised of multiple sets of cameras and projectors, as shown in Fig. 1. The system's characterisation is carried out using a checkerboard which is moved manually in the measurement volume and images are captured for different orientations. These images are then used to determine the intrinsic parameters of the cameras. Sinusoidally varying phase-stepped fringe patterns are generated using a computer and projected onto the checkerboard. The absolute phase is acquired through temporal phase unwrapping that relies on a combined phase-stepped and binary coded method, described in section 2.1. The retrieved phase maps are used to determine the extrinsic parameters and the global frame of reference discussed in sections 2.1 and 2.2.

The details of the geometric characterisation procedure are discussed in detail in the following sections.

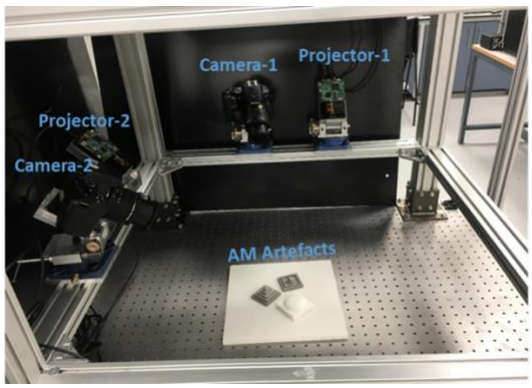

Fig. 1 Multi-view fringe projection system

2.1. Geometric characterisation

Camera characterisation is a well-developed field [8-9, 13-14], and in general, a camera is described by the pinhole model [9]. The relationship between a point on the object and its projection on the image sensor can be represented as

$$S^c I^c = A^c [R^c, T^c] X^w = A^c M^c X^w, \tag{1}$$

where $I^c = [u^c, v^c, 1]^T$ is the homogeneous coordinate of the image point in the image coordinate system, $X^w = [x^w, y^w, z^w, 1]^T$ is the homogeneous point coordinate in the world coordinate system, S^c is the scaling factor, R^c *and* T^c are extrinsic rotational and translational matrices respectively, $[R^c, T^c]$ is the extrinsic parameter matrix, defined as M^c in equation (1), while A^c is the intrinsic parameter matrix, represented as

$$A^c = \begin{pmatrix} \alpha^c & \gamma^c & u_0^c \\ 0 & \beta^c & v_0^c \\ 0 & 0 & 1 \end{pmatrix}, \tag{2}$$

where, α^c and β^c are the focal lengths along $[u^c, v^c]$ of the image plane, $[u_0^c, v_0^c]$ is the principal point and γ^c is the skewness.

The camera characterisation is performed using a standard checkerboard (4 mm square) which is placed at several different positions in the measurement volume, and images are captured by projecting a plain white image pattern onto the checkerboard.

Table 1. Geometric characterisation results for the cameras

Parameter	Outcome
Intrinsic parameter for camera 1 (A_1^c)	$\begin{pmatrix} 9326.3 & 0 & 2281.7 \\ 0 & 9234.1 & 1524 \\ 0 & 0 & 1 \end{pmatrix}$
Intrinsic parameter for camera 2 (A_2^c)	$\begin{pmatrix} 10545 & 0 & 2240 \\ 0 & 10833 & 1358 \\ 0 & 0 & 1 \end{pmatrix}$

Table 2. Geometric characterisation results for the projectors

Parameter	Outcome
Intrinsic parameter for projector 1 (A_1^p)	$\begin{pmatrix} 1509.3 & 0 & 314.2 \\ 0 & 4855.7 & 612.6 \\ 0 & 0 & 1 \end{pmatrix}$
Intrinsic parameter for projector 2 (A_2^p)	$\begin{pmatrix} 863.2 & 0 & 358.9 \\ 0 & 1479.2 & 456.9 \\ 0 & 0 & 1 \end{pmatrix}$

The intrinsic (A_1^c, A_2^c) parameters for both the cameras are determined using an image processing algorithm. The measured parameters are listed in Table 1.

The extrinsic parameters of the cameras and projectors are determined by projecting fringes and the absolute phase map information. A phase map for the multi-view system is obtained by projecting a set of sinusoidal phase-stepped and binary fringe patterns. The binary fringes are used to evaluate the fringe order, which is the key parameter in temporal phase unwrapping [18]. For *N*-step phase shifted patterns, the intensity of the i^{th} image with a phase shift of δ_i can be represented as

$$I_i(x,y) = I'(x,y) + I''(x,y)\cos(\varphi(x,y) + \delta_i), \tag{3}$$

where $I'(x,y)$ is the average intensity, $I''(x,y)$ is the modulated intensity, $\varphi(x,y)$ is the phase and $\delta_i = (2\pi i/N)$ is the phase difference. The phase can be written as

$$\varphi(x,y) = -\tan^{-1}\left(\frac{\sum_{i=1}^{N} I_i \sin\delta_i}{\sum_{i=1}^{N} I_i \cos\delta_i}\right). \tag{4}$$

Zhang and Huang [19] showed that a camera can be used to capture images for the projector by transforming the camera image pixel coordinates into projector image pixel coordinates.

A set of horizontal and vertical phase-stepped patterns are projected onto the checkerboard and images are captured at several different orientations by moving the checkerboard manually in the measurement volume. For each characterisation pose, the projector coordinates are determined from the camera coordinates using the one-one correspondence established through the phase maps [10]. Table 2 shows the projector parameters. Mathematically, the transformation relation can be represented as

$$u^p = \varphi_h(u^c, v^c)\ P/2\pi, \tag{5}$$

$$v^p = \varphi_v(u^c, v^c)\ P/2\pi, \tag{6}$$

where (u^p, v^p) are the image coordinates of the projector, (φ_h, φ_v) are the horizontal and vertical phase values, P is the fringe pitch which corresponds to the number of pixels per fringe period.

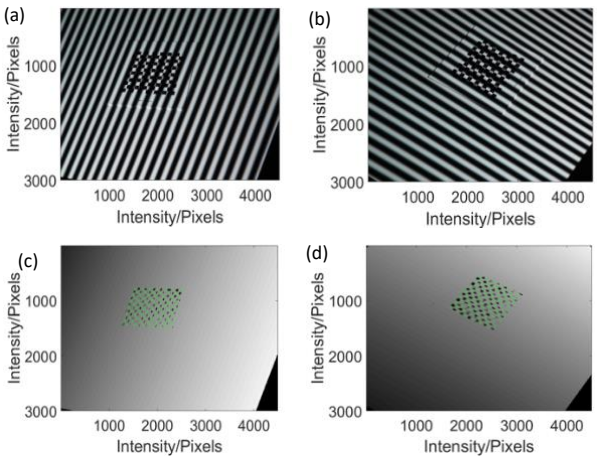

Fig. 2 Fringes projected on the checkerboard and captured by two different cameras from different perspectives. (a-b) Original images, (c-d) corresponding phase maps with the detected checkerboard points being projected back.

Fig. 2 shows the fringes projected onto the checkerboard pattern and the corresponding phase maps with square centres detected for one orientation. Fig. 3 depicts the reprojection errors for the cameras and projectors for six different positions. The reprojection errors are less than half a pixel, showing that the geometric characterisation was successful.

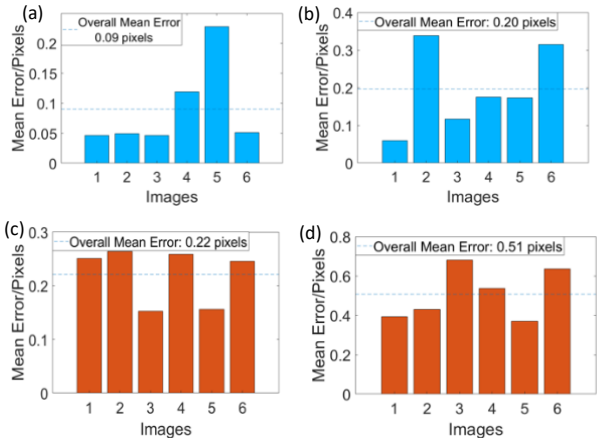

Fig. 3 Reprojection errors per image. (a) Camera 1, (b) Camera 2, (c) Projector 1, (d) Projector 2.

2.2. Global frame of reference

The initial steps (mentioned in section 2.1) determine the intrinsic and extrinsic parameters for each individual camera and projector. The location and orientation of each camera and projector are automatically defined in the same global reference frame. The transformation from the image coordinates to the three-dimensional world coordinates can be achieved through triangulation. Each combination of camera and projector is considered as a stereo pair, with the transformation relationship given by

$$S^c I^c = A^c[R^c, T^c]X^w, \tag{7}$$

$$S^p I^p = A^p[R^p, T^p]X^w, \tag{8}$$

where I^c and I^p are the homogeneous coordinates of the image point in the image coordinate system of the camera and projector respectively, X^w is the homogeneous point coordinate in the world coordinate system, (A^c, A^p) are the intrinsic, (R^c, R^p) the rotational and (T^c, T^p) the translational parameters for the camera and projector. The global relationship between the camera and projector views is obtained by a plane in the common field-of-view of both the cameras and projectors. The homography matrices H^c and H^p for the camera and projector correspond to the projection matrices given equations (7) and (8) and are represented as

$$H^c = A^c[R^c, T^c] = \begin{pmatrix} h_{11}^c & h_{12}^c & h_{13}^c & h_{14}^c \\ h_{21}^c & h_{22}^c & h_{23}^c & h_{24}^c \\ h_{31}^c & h_{32}^c & h_{33}^c & h_{34}^c \end{pmatrix}, \tag{9}$$

$$H^p = A^p[R^p, T^p] = \begin{pmatrix} h_{11}^p & h_{12}^p & h_{13}^p & h_{14}^p \\ h_{21}^p & h_{22}^p & h_{23}^p & h_{24}^p \\ h_{31}^p & h_{32}^p & h_{33}^p & h_{34}^p \end{pmatrix}. \tag{10}$$

The world coordinates can be acquired based on the triangulation equation given by

$$\begin{pmatrix} x \\ y \\ z \end{pmatrix} = \begin{pmatrix} h_{11}^c - u^c h_{31}^c & h_{12}^c - u^c h_{32}^c & h_{13}^c - u^c h_{33}^c \\ h_{21}^c - v^c h_{31}^c & h_{22}^c - v^c h_{32}^c & h_{23}^c - v^c h_{33}^c \\ h_{11}^p - u^p h_{31}^p & h_{12}^p - u^p h_{32}^p & h_{13}^p - u^p h_{33}^p \end{pmatrix}^{-1} \times \begin{pmatrix} u^c h_{34}^c - h_{14}^c \\ v^c h_{34}^c - h_{24}^c \\ u^p h_{34}^p - h_{14}^p \end{pmatrix}. \tag{11}$$

3. Experiments

The experimental setup for the multi-view fringe projection system (Fig. 1) is comprised of two DSLR cameras (Nikon D3500, 4496 × 3000 pixels), two digital light processing (DLP) projectors (DLPC300 Texas Instruments) with a digital micromirror device (608 × 680 pixels). In the multi-view fringe projection system, the two sets of cameras and projectors are mounted on a rigid metal mount to alleviate mechanical vibration. The tested object is placed approximately 50 cm from the projectors. The projector's digital micromirror device chip is used to project the images onto the tested object. The overlap between the projectors is overcome by only displaying fringes through a single projector at any one time.

3.1. Results

The geometric characterisation of the multi-view fringe projection system is carried out by using a checkerboard and capturing images at different orientations, as discussed in section 2.1 to 2.2. To further estimate the system's characterisation accuracy, the three-dimensional measurement of an AM artefact is performed using a set of phase-stepped sinusoidal fringes and binary coded fringes. Since the multi-view system with two sets of cameras and projectors that share the same frame of reference, four individual point clouds have been acquired for two different projections and from two separate perspectives, as shown in Fig. 4 (a-d).

Fig. 5(a) shows the three-dimensional reconstructed results of a hemisphere artefact (Nylon-12, (60 × 60 × 20) mm) with a single camera-projector based fringe projection system. Fig. 5(b) depicts the point cloud by combining the reconstruction results from different perspectives.

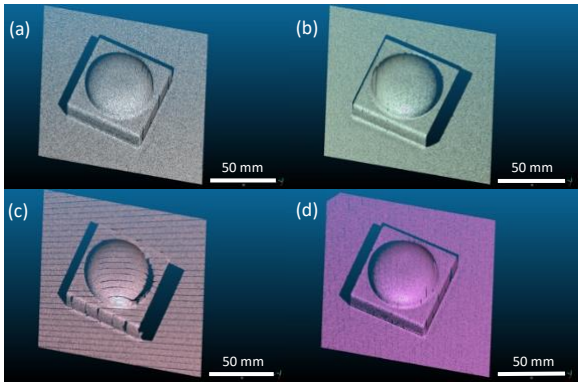

Fig. 4 Three-dimensional reconstruction results from different perspectives. (a) Projector 1-Camera 1, (b) Projector 1-Camera 2, (c) Projector 2-Camera 1, (d) Projector 2-Camera 2

Compared to the single view system, the multi-view system provides a better performance and can overcome the self-occlusion and shadowing effect of the AM part. The reconstruction result in Fig. 5(b) is more complete as there is no gap on the sides of the artefact. There is also no obvious offset between the two views which shows the consistency of the measurement data.

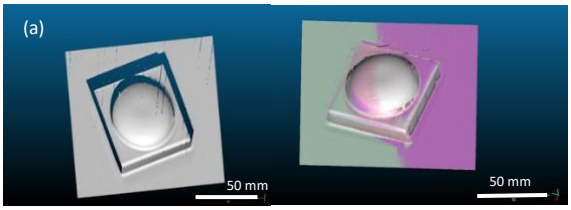

Fig. 5 Three-dimensional reconstruction results for a hemisphere (60×60×20 mm) Nylon-12 artefact. (a) Point cloud from a single-camera projector, (b) point cloud from two sets of cameras and projectors

However, the full three-dimensional form of the measured AM artefact requires projections from more positions. The multi-view system is tested with two sets of cameras and projectors and can be generalised for *N* cameras and projectors using the same algorithmic solution. Future work will focus on the global optimisation of the geometric characterisation for the multi-view fringe projection system and improving its speed and accuracy.

4. Conclusions

In this paper, an automated geometric characterisation approach for a cost-effective -view fringe projection system has been presented. The method uses a checkerboard to characterise the system and determine the intrinsic and extrinsic parameters of all the cameras and projectors. The phase information from the phase-stepped fringes is used to establish the global reference frame by automated image processing and parameter optimisation. The geometric characterisation method is implemented, and the multi-view system has been used to measure an AM artefact. The three-dimensional reconstruction results from the different views are registered with the ICP algorithm. The reconstructed results for a multi-view system alleviated the limitations of a single view system, mainly associated with occlusions, shading and high slope angles.

Acknowledgements

This research was funded by The EU Framework Programme for Research and Innovation - Horizon 2020 - Grant Agreement No 721383 within the PAM^2 (Precision Additive Metal Manufacturing) research project and by the Engineering and Physical Sciences Research Council [EPSRC Grant numbers EP/M008983/1, EP/L016567/1].

References

[1] Nguyen H, Nguyen D, Wang Z, Kieu H and Minh Le 2015 Real-time, high-accuracy 3D imaging and shape measurement *Appl. Opt.* **54** A9-A17
[2] Jiang C, Jia S, Dong J, Bao Q, Yang J, Lian Q, and Li D 2015 Multi-frequency color-marked fringe projection profilometry for fast 3D shape measurement of complex objects *Opt. Express* **23** 24152-24162
[3] Zhang S 2018 High-speed 3D shape measurement with structured light methods: A review *Opt. Lasers Eng,* **106** 119-131
[4] Yen H-N, Tsai D-M, and J-Y Yang 2006 Full-field 3-D measurement of solder pastes using LCD-based phase shifting techniques *IEEE Trans. Electron. Packag. Manuf.* **29** 50-57
[5] Chen L-C and Huang C-C 2005 Miniaturized 3D surface profilometer using digital fringe projection *Meas. Sci. Technol.* **16** 1061–1062
[6] Lin C.-h et al., 2005 Fringe projection measurement system in reverse engineering *J. Shanghai Univ*. **9** 153-158
[7] Zhang Z H Y 2004 Camera calibration with one- dimensional objects *IEEE Trans. Pattern Anal. Mach. Intell.* **26** 892-899
[8] Gai S, Da F and Fang X 2016 A novel camera calibration method based on polar coordinate *PLoS One* **11** e0165487
[9] Feifei G *et al* 2015 Camera calibration based on the back projection process *Meas. Sci. Technol.* **26** 125004
[10] Gai S, Daand F, Tang M 2019 A flexible multi-view calibration and 3D measurement method based on digital fringe projection *Meas. Sci. Technol.* **30** 025203
[11] Deetjen M E and Lentink D 2018 Automated calibration of multi-camera-projector structured light systems for volumetric high-speed 3D surface reconstructions *Opt. Express* **25** 33278-33304
[12] Huang Z Xi J, Yu Y, and Guo Q *2*015 Accurate projector calibration based on a new point-to-point mapping relationship between the camera and projector images *Appl. Opt.* **54** 347–356
[13] Zhang Z H Y 2000 A flexible new technique for camera calibration *IEEE Trans. Pattern Anal. Mach. Intell.* **22** 1330–1334
[14] Lu R S and Li Y F 2004 A global calibration method for large-scale multi-sensor visual measurement systems *Sens. Actuators* A **116** 384–393
[15] Liu Z GuangjunZhang G, Wei Z, Sun J 2011 Novel calibration method for non-overlapping multiple vision sensors based on 1D target *Opt. Lasers Eng.* **49** 570–577
[16] Zhao H, Chen Y and Shibasaki R 2007 An efficient extrinsic calibration of a multiple laser scanners and cameras' sensor system on a mobile platform *Intelligent Vehicles Symp.* (IEEE) 422–427
[17] Du S, Xu Y, Wan T, Hu H, Zhang S, Xu G, Zhang X 2017 Robust iterative closest point algorithm based on global reference point for rotation invariant registration *PLoS ONE* **12** e0188039
[18] Sansoni G, Carocci M and Rodella R 1999 Three-dimensional vision based on a combination of gray-code and phase-shift light projection: analysis and compensation of the systematic errors *Appl. Opt.* **38** 6565-6573
[19] Zhang S and Huang P S 2006 Novel method for structured light system calibration *Opt. Eng.* **45** 083601